CHAPTER TWO

A Phenomenological Approach to Diode Lasers

2.1 INTRODUCTION

In this chapter we attempt to develop an engineering toolbox of diode laser properties based largely upon phenomenological arguments. In the course of this development, we make heavy reference to several appendices for a review of some of the underlying physics.

The chapter begins by developing a rate equation model for the flow of charge into double-heterostructure active regions and its subsequent recombination. Some of this electron–hole recombination generates photons by spontaneous emission. This incoherent light is important in LEDs, and a section is devoted to deriving the relevant equations governing LED operation.

Sections 2.4 through 2.6 provide a systematic derivation of the dc light-current characteristics of diode lasers. First, the rate equation for photon generation and loss in a laser cavity is developed. This shows that only a small portion of the spontaneously generated light contributes to the lasing mode. Most of it comes from the stimulated recombination of carriers. All of the carriers that are stimulated to recombine by light in a certain mode contribute more photons to that same mode. Thus, the stimulated carrier recombination/photon generation process is a *gain* process. The threshold gain for lasing is studied next, and it is found to be the gain necessary to compensate for cavity losses. The current required to reach this gain is called the threshold current, and it is shown to be the current necessary to supply carriers for the unproductive nonradiative and spontaneous recombination processes, which clamp at their threshold value as more current is applied. Above threshold, all additional injected carriers recombining in the active region are shown to contribute to photons in the lasing mode. A fraction escape through the mirrors; others are absorbed by optical losses in the cavity.

The next section deals with the modulation of lasers. Here for the first time we solve the rate equations for a modulated current. Under small-signal modulation, the rate equations for carriers and photons are found to be analogous to the differential equations that describe the current and voltage in an *RLC* circuit. Thus, the optical modulation response is found to have a resonance and to fall off rapidly above this frequency.

Finally, this chapter reviews techniques for characterizing real lasers. These techniques can be used to extract the important device parameters used in the theoretical derivations. They also provide practical terminal parameters that are useful in the design of optoelectronic circuits.

2.2 CARRIER GENERATION AND RECOMBINATION IN ACTIVE REGIONS

The text accompanying Figs. 1.4, 1.5, and 1.13 considers the current injected into the terminals of a diode laser or LED, and suggests it is desirable to have all of it contribute to electrons and holes which recombine in the active region. However, in practice only a fraction, η_i, of the injected current, I, does contribute to such carriers. In Fig. 2.1 we again illustrate the process of carrier injection into a double-heterostructure active region using a somewhat more accurate sketch of the energy gap vs. depth into the substrate.

Since the definitions of the active region and the internal quantum efficiency, η_i, are so critical to further analysis, we highlight them here for easy reference.

> *Active region: the region where recombining carriers contribute to useful gain and photon emission.*

The active region is usually the lowest bandgap region within the depletion region of a *pin* diode for efficient injection. However, it occasionally is convenient to include some of the surrounding intermediate bandgap regions. Also in this definition, *useful* is the operative word. There may be photon emission and even gain at some undesired wavelength elsewhere in the device.

> *Internal quantum efficiency, η_i: the fraction of terminal current that generates carriers in the active region.*

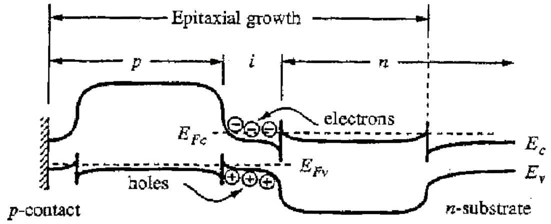

FIGURE 2.1 Band diagram of forward biased double-heterostructure diode.

It is important to realize that this definition includes *all* of the carriers that are injected into the active region, not just carriers that recombine radiatively at the desired transition energy. This definition is oftentimes misstated in the literature.

We also will specifically analyze active regions that are undoped or lightly doped, so that under high injection levels relevant to LEDs and lasers, charge neutrality dictates that the electron density equals the hole density, i.e., $N = P$ in the active region. Thus, we can greatly simplify our analysis by specifically tracking only the electron density, N.

The carrier density in the active region is governed by a dynamic process. In fact, we can compare the process of establishing a certain steady-state carrier density in the active region to that of establishing a certain water level in a reservoir which is being simultaneously filled and drained. This is shown schematically in Fig. 2.2. As we proceed, the various filling (generation) and drain (recombination) terms illustrated will be defined. The current leakage illustrated in Fig. 2.2 contributes to reducing η_i and is created by possible shunt paths around the active region. The carrier leakage, R_l, is due to carriers "splashing" out of the active region (by thermionic emission or by lateral diffusion if no lateral confinement exists) before recombining. Thus, this leakage contributes to a loss of carriers in the active region that could otherwise be used to generate light.

For the DH active region, the injected current provides a generation term, and various radiative and nonradiative recombination processes as well as carrier leakage provide recombination terms. Thus, we can write the rate equation,

$$\frac{dN}{dt} = G_{gen} - R_{rec}, \tag{2.1}$$

where G_{gen} is the rate of injected electrons and R_{rec} is the rate of recombining electrons per unit volume in the active region. Since there are $\eta_i I/q$ electrons per second being injected into the active region,

$$G_{gen} = \frac{\eta_i I}{qV}, \tag{2.2}$$

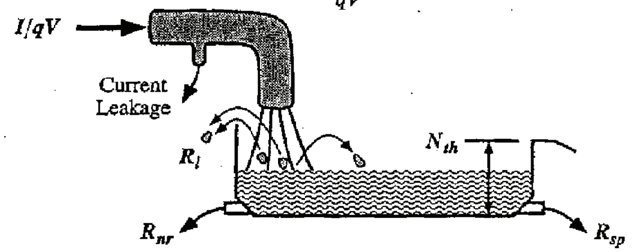

FIGURE 2.2 Reservoir with continuous supply and leakage as an analog to a DH active region with current injection for carrier generation and radiative and nonradiative recombination (LED or laser below threshold).

where V is the volume of the active region. For example, if a current of $I = 20$ mA is flowing into the laser's terminals, a fraction $\eta_i = 80\%$ of the carriers are injected into the active region, and if the active volume is 100 μm^3, then $G_{gen} = 10^{27}$ electrons/s-cm^3. Or, 10^{18} cm^{-3} electrons are injected in 1 ns.

The recombination process is a bit more complicated, since several mechanisms must be considered. As introduced in Fig. 1.3, there is a spontaneous recombination rate, R_{sp}, and a nonradiative recombination rate, R_{nr}. And as depicted in Fig. 2.2, a carrier leakage rate, R_l, must sometimes be included if the transverse and/or lateral potential barriers are not sufficiently high (see Appendix 2 for a discussion of R_l). Finally, under the right conditions, a net stimulated recombination, R_{st}, including both stimulated absorption and emission, is important. Thus, we can write

$$R_{rec} = R_{sp} + R_{nr} + R_l + R_{st}. \tag{2.3}$$

The first three terms on the right refer to the natural or unstimulated carrier decay processes. The fourth one, R_{st}, requires the presence of photons. It is common to describe the natural decay processes by a *carrier lifetime*, τ. In the absence of photons or a generation term, the rate equation for carrier decay is just, $dN/dt = N/\tau$, where $N/\tau \equiv R_{sp} + R_{nr} + R_l$, by comparison to Eq. (2.3). This rate equation defines τ. Also, as mentioned in Chapter 1, this natural decay can be expressed in a power series of the carrier density, N, since each of the terms depends upon the existence of carriers. Thus, we can rewrite Eq. (2.3) in several ways.

$$R_{rec} = R_{sp} + R_{nr} + R_l + R_{st}, \tag{2.3a}$$

$$R_{rec} = \frac{N}{\tau} + R_{st}, \tag{2.3b}$$

$$R_{rec} = BN^2 + (AN + CN^3) + R_{st}, \tag{2.3c}$$

where as the grouping suggests in (2.3c), it has been found that $R_{sp} \sim BN^2$ and $R_{nr} + R_l \sim (AN + CN^3)$. The coefficient B is called the *bimolecular recombination coefficient*, and it has a magnitude, $B \sim 10^{-10}$ cm^3/s for most AlGaAs and InGaAsP alloys of interest. We also note that the carrier lifetime, τ, is not independent of N in most circumstances.

Thus, so far we can write our carrier rate equation in several equivalent ways. We shall deal with R_{st} a little later, but using Eq. (2.3b), our carrier rate equation may be expressed as

$$\frac{dN}{dt} = \frac{\eta_i I}{qV} - \frac{N}{\tau} - R_{st}. \tag{2.4}$$

In the absence of a large photon density, such as in a laser well below threshold or in most LEDs, it can be shown that R_{st} can be neglected. Figure 2.2 illustrates each of these terms in our reservoir analogy, explicitly showing "leaks" R_{sp}, R_{nr}, and R_l for N/τ.

2.3 SPONTANEOUS PHOTON GENERATION AND LEDs

Before proceeding to the consideration of lasers, where R_{st} will become a dominant term above threshold, let us first try to gain some understanding of the situation where the photon density is relatively low, such as in an LED where no feedback is present to provide for the build-up of a large photon density. This case is actually similar to a laser below threshold, in which the gain is insufficient to compensate for cavity losses, and generated photons do not receive net amplification.

The spontaneous photon generation rate per unit volume is exactly equal to the spontaneous electron recombination rate, R_{sp}, since by definition every time an electron–hole pair recombines radiatively, a photon is generated. (Again, N equals the density of electron–hole pairs as well as electrons for relatively light doping). Under *steady-state* conditions ($dN/dt = 0$), the generation rate equals the recombination rate, i.e., from Eqs. (2.2) and (2.3), with $R_{st} \approx 0$,

$$\frac{\eta_i I}{qV} = R_{sp} + R_{nr} + R_l. \tag{2.5}$$

The spontaneously generated optical power, P_{sp}, is obtained by multiplying the number of photons generated per unit time per unit volume, R_{sp}, by the energy per photon, $h\nu$, and the volume of the active region, V. We could solve Eq. (2.5) for R_{sp}, but since the exact dependence of $R_{nr} + R_l$ on I is unknown, this leads only to a parametric equation. The conventional approach is to bury this problem by defining a *radiative efficiency, η_r*, where

$$\eta_r = \frac{R_{sp}}{R_{sp} + R_{nr} + R_l}. \tag{2.6}$$

We must not forget that η_r usually depends upon carrier density somewhat. Then, from Eqs. (2.5) and (2.6),

$$P_{sp} = h\nu V R_{sp} = \eta_i \eta_r \frac{h\nu}{q} I. \tag{2.7}$$

The product of $\eta_i \eta_r$ is sometimes referred to as the LED internal efficiency. However, we shall *not* use this definition here, since it can lead to serious confusion when we move on to lasers. As we shall see, only η_i appears in the laser output power, and we have called it alone the internal efficiency.

If we are interested in how much power the LED emits into some receiving aperture, P_{LED}, we must further multiply P_{sp} by the *net collection efficiency, η_c*, experienced in transmitting photons out of the semiconductor and into this aperture. This is typically relatively low (<10%) for most LEDs, because the light is emitted in all directions, and much of it is totally reflected at the semiconductor–air interface. This situation is illustrated in Fig. 2.3.

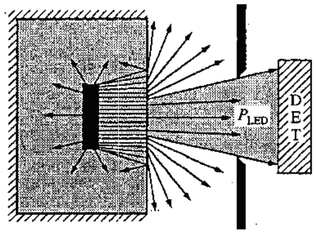

FIGURE 2.3 Schematic of LED showing how only a small portion of the generated light reaches a desired detector.

As indicated by Fig. 2.3 much of the light is reflected back toward the active region rather than being coupled out of the semiconductor chip. A possible consequence is the regeneration of new carriers by the reabsorption of this light. In properly designed LEDs this "photon recycling" can greatly increase their efficiency, yielding an effective $\eta_c > 10\%$.

In any event, the product of the three efficiencies (fraction of carriers injected into the active region, fraction of these recombining radiatively, and the fraction of those usefully coupled out) gives the *external LED quantum efficiency*, η_{ex}. That is,

$$P_{LED} = \eta_c \eta_i \eta_r \frac{h\nu}{q} I = \eta_{ex} \frac{h\nu}{q} I. \tag{2.8}$$

Thus, ignoring the slight dependence of η_{ex} on I, we see that the power coupled from an LED is directly proportional to the drive current. The external LED quantum efficiency, η_{ex}, is the number of photons coupled to the receiving aperture per electron flowing into the LED.

The frequency response of the LED can also be derived from the carrier rate equation (2.4), with $R_{st} \approx 0$. We shall use the theorem that the Fourier transform of the impulse response in the time domain gives the frequency response. An impulse of current is simply a quantity of charge, which will establish an initial condition of $N(t = 0^+) = N_i$. For $t > 0$, the rate equation can be written as

$$\frac{dN}{dt} = -\frac{N}{\tau} = -AN - BN^2 - CN^3. \tag{2.9}$$

With the polynomial expansion of the recombination rate, we are reminded that the carrier lifetime, τ, is generally a function of the carrier density. If it were independent of N, the solution would be a simple exponential decay, and the frequency response would be analogous to that of a simple RC circuit in which the 3 dB cutoff frequency, $\omega_c = 1/\tau$. In order for τ to be constant: (1) the cubic term must be negligible and (2) either the linear term, AN, must dominate (not good, since this represents nonradiative recombination) or the active region must be heavily doped, such that the BN^2 term which really equals BNP, can be written as $(BP_d)N$. That is, the p-type doping level, P_d, must be greater than the injection level, N, so that $P_d + P \approx P_d$. Under these conditions, then, the time response is just a simple exponential decay,

$$N(t) = N_i e^{-t/\tau}, \tag{2.10}$$

and the frequency response is a Lorentzian function,

$$N(\omega) = \frac{N(0)}{1 + j\omega\tau}, \tag{2.11}$$

which drops to 0.707 $N(0)$ at $\omega\tau = 1$. For $R_{sp} \approx (BP_d)N$, the power out, P_{LED}, which is proportional to R_{sp}, will also have the same frequency response. The other cases are left as exercises for the reader, but it should be clear that the cutoff frequency will be reduced if the carrier lifetime is increased.

2.4 PHOTON GENERATION AND LOSS IN LASER CAVITIES

For the diode laser, we must now further investigate the nature of the net stimulated recombination rate, R_{st}, in generating photons as well as the effect of the resonant cavity in storing photons. In analogy with Section 2.2, we wish to construct a rate equation for the *photon density*, N_p, which includes the photon generation and loss terms. We shall use the subscript p to indicate that variables are referring to photons.

A main difference between the laser and LED, discussed in Section 2.3 above, is that we only consider light emission into a single mode of the resonant cavity in the laser. Since there are typically thousands of possible optical modes in a diode laser cavity, only a small fraction of R_{sp} contributes to the photon generation rate for a particular mode. Appendix 4 discusses the possible optical modes of a resonant cavity using some of the results of Appendix 3. Note that the number of effective modes in a small vertical-cavity laser can be much fewer, typically dozens rather than thousands.

The main photon generation term above threshold (the regime of interest in lasers) is R_{st}. Every time an electron–hole pair is stimulated to recombine, another photon is generated. However, as indicated in Fig. 2.4, since the cavity volume occupied by photons, V_p, is usually larger than the active region volume occupied by electrons, V, the photon *density* generation rate will be $[V/V_p]R_{st}$ not just R_{st}. This electron–photon overlap factor, V/V_p, is generally referred to as the *confinement factor*, Γ. Sometimes it is convenient to introduce an effective thickness, width, and length that contains the photons, d_{eff}, w_{eff}, and L, respectively. That is, $V_p = d_{eff} w_{eff} L$. Then, if the active region has dimensions, d, w, and L_a, the confinement factor can be expressed as, $\Gamma = \Gamma_x \Gamma_y \Gamma_z$, where $\Gamma_x = d/d_{eff}$, $\Gamma_y = w/w_{eff}$, and $\Gamma_z = L_a/L$. Appendix 5 puts the derivation of Γ on a more rigorous foundation, pointing out that Γ_z is subject to an enhancement factor for $L_a \lesssim \lambda$.

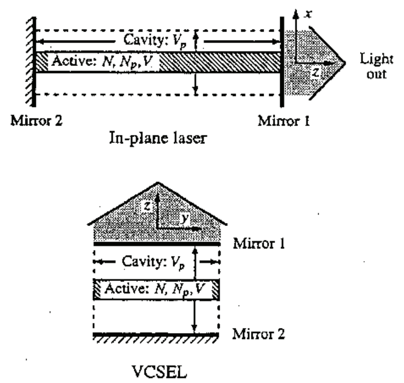

FIGURE 2.4 Schematics of in-plane and vertical-cavity lasers illustrating the active (cross-hatched) and cavity (within dashed lines) volumes as well as the coordinate systems.

Photon loss occurs within the cavity due to optical absorption and scattering out of the mode, and it also occurs at the output coupling mirror where a portion of the resonant mode is usefully coupled to some output medium. These losses will be quantified in the next section, but for now we can characterize the net loss by a *photon (or cavity) lifetime*, τ_p, analogous to how we handled electron losses above. A first version of the photon rate equation takes the form:

$$\frac{dN_p}{dt} = \Gamma R_{st} + \Gamma \beta_{sp} R_{sp} - \frac{N_p}{\tau_p}, \tag{2.12}$$

where β_{sp} is the *spontaneous emission factor*. As indicated in Appendix 4 for uniform coupling to all modes, β_{sp} is just the reciprocal of the number of optical modes in the bandwidth of the spontaneous emission. As also indicated by Eq. (2.12), in the absence of generation terms, the photons decay exponentially with a decay constant of τ_p. Again, this is really the definition of τ_p.

Equations (2.4) and (2.12) are two coupled equations that can be solved for the steady-state and dynamic responses of a diode laser. However, in their present form there are still several terms that need to be written explicitly in terms of N and N_p before such solutions are possible. First, we shall consider R_{st}.

R_{st} represents the photon-stimulated net electron–hole recombination which generates more photons. This is a *gain* process for photons. As illustrated in Fig. 1.3 and discussed more fully in Appendix 6, the net effect of the upward and downward electronic transitions, corresponding to stimulated absorption and emission of photons, respectively, are included. In Fig. 2.5 we show the growth of a photon density from an incoming value of N_p to an exiting value of $N_p + \Delta N_p$ as it passes through a small length, Δz, of active region. Without loss of generality, but for simplicity, we assume full overlap between the active region and the photon field, i.e., $\Gamma = 1$. As shown, we can also describe this growth in terms of a *gain per unit length*, g, by

$$N_p + \Delta N_p = N_p e^{g\Delta z}. \tag{2.13}$$

If Δz is sufficiently small, $\exp(g\Delta z) \approx (1 + g\Delta z)$. Also, using the fact that $\Delta z = v_g \Delta t$, where v_g is the group velocity, we find that, $\Delta N_p = N_p g v_g \Delta t$. That is, the generation term for dN_p/dt is given by

$$\left(\frac{dN_p}{dt}\right)_{gen} = R_{st} = \frac{\Delta N_p}{\Delta t} = v_g g N_p. \tag{2.14}$$

Thus, we can now rewrite the carrier and photon density rate equations,

$$\frac{dN}{dt} = \frac{\eta_i I}{qV} - \frac{N}{\tau} - v_g g N_p, \tag{2.15}$$

$$\frac{dN_p}{dt} = \Gamma v_g g N_p + \Gamma \beta_{sp} R_{sp} - \frac{N_p}{\tau_p}. \tag{2.16}$$

Of course, we still have not made all the substitutions necessary to directly solve the two equations simultaneously. In Appendix 6 it is suggested that the gain as a function of carrier density can be approximated by a straight line, at least under small-signal conditions. That is,

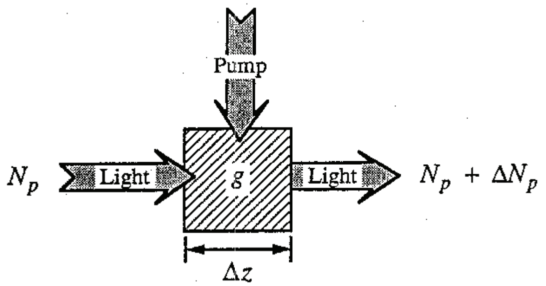

FIGURE 2.5 Definition of gain in terms of the increase in photon number across a small segment of gain material.

$$g \approx a(N - N_{tr}), \tag{2.17}$$

where a is the *differential gain*, $\partial g/\partial N$, and N_{tr} is a *transparency carrier density*. (Actually, a logarithmic function fits the gain better over a wider range of N, as we shall detail in Chapter 4.) Of course, we also know that N/τ can be replaced by the polynomial $AN + BN^2 + CN^3$, where the terms estimate defect, spontaneous (R_{sp}), and Auger recombination, respectively. Nevertheless, we shall leave the rate equations in the general form of Eqs. (2.15) and (2.16) for future reference.

2.5 THRESHOLD OR STEADY-STATE GAIN IN LASERS

In Section 2.4, we characterized the cavity loss by a photon decay constant or lifetime, τ_p. Here, we wish to explicitly express τ_p in terms of the losses associated with optical propagation along the cavity and the cavity mirrors. Also, we wish to show that the net loss of some mode gives the value of net gain required to reach the lasing threshold.

As shown in Appendix 3 and discussed in Chapter 1, the optical energy of a modern diode laser propagates in a dielectric waveguide mode which is confined both transversely and laterally as defined by a normalized transverse electric field profile, $U(x, y)$. In the axial direction this mode propagates as $\exp(-j\tilde{\beta}z)$, where $\tilde{\beta}$ is the complex propagation constant which includes any loss or gain. Thus, the time- and space-varying electric field can be written as

$$\mathscr{E} = \hat{\mathbf{e}}_y E_0 U(x, y) e^{j(\omega t - \tilde{\beta} z)}, \tag{2.18}$$

where $\hat{\mathbf{e}}_y$ is the unit vector indicating TE polarization and E_0 is the magnitude of the field. The complex propagation constant, $\tilde{\beta}$, includes the incremental *transverse modal gain*, $\langle g \rangle_{xy}$ and *internal modal loss*, $\langle \alpha_i \rangle_{xy}$. That is,

$$\tilde{\beta} = \beta + j\beta_i = \beta + \frac{j}{2}(\langle g \rangle_{xy} - \langle \alpha_i \rangle_{xy}), \tag{2.19}$$

where the real part of $\tilde{\beta}$; $\beta = 2\pi\bar{n}/\lambda$, and $\bar{n}$ is an effective index of refraction for the mode, also defined in Appendix 3. As shown in Appendix 5, the transverse modal gain, $\langle g \rangle_{xy}$, and loss, $\langle \alpha_i \rangle_{xy}$, are found from weighted averages of the gain and loss, respectively, across the mode shape, $U(x, y)$. Both are related to power; thus, the factor of $\frac{1}{2}$ in this equation for the amplitude propagation coefficient. From Appendix 5, we can let $\langle g \rangle_{xy} = \Gamma_{xy} g$, where Γ_{xy} is the transverse confinement factor, if $g(x, y)$ is constant across the active region and

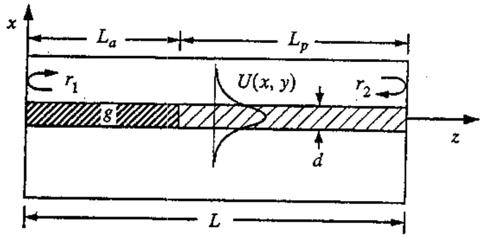

FIGURE 2.6 Generic laser cavity cross section showing active and passive sections (no impedance discontinuity assumed) and the guided-mode profile.

zero elsewhere. This is generally valid for in-plane lasers, but not for VCSELs. Also, for notational convenience, we shall let $\langle \alpha_i \rangle_{xy} = \alpha_i$.

As illustrated in Fig. 2.6, most laser cavities can be divided into two general sections: an active section of length L_a and a passive section of length L_p. Also, g and α_i will clearly be different in these two sections. In the passive section, by definition $g = 0$, and α_i can be given a second subscript to designate its location. The propagating mode is reflected by end mirrors, which have amplitude reflection coefficients of r_1 and r_2, respectively, to provide a resonant cavity. The amount transmitted is potentially useful output.

In order for a mode of the laser to reach threshold, the gain in the active section must be increased to the point where all the propagation and mirror losses are compensated, so that the electric field exactly replicates itself after one round-trip in the cavity. Equivalently, we can unravel the round-trip to lie along the z-axis and require that $\mathscr{E}(z = 2L) = \mathscr{E}(z = 0)$, provided we insert the mode reflection coefficients at $z = 0$ and $z = L$. As a consequence of inserting these boundaries into Eq. (2.18), we obtain

$$r_1 r_2 e^{-2j\tilde{\beta}_{ath}L_a} e^{-2j\tilde{\beta}_{pth}L_p} = 1. \tag{2.20}$$

The subscript th denotes that this characteristic equation only defines the threshold value of $\tilde{\beta}$. (In Chapter 3 we shall take a more basic approach to obtain this same characteristic equation.) Using Eq. (2.19), we can break the complex Eq. (2.20) into two equations for its magnitude and phase. For the magnitude,

$$r_1 r_2 e^{(\Gamma_{xy} g_{th} - \alpha_{ia})L_a} e^{-\alpha_{ip} L_p} = 1, \tag{2.21}$$

where we have chosen reference planes to make the mirror reflectivities real. Solving for $\Gamma_{xy} g_{th} L_a$ we obtain

$$\Gamma_{xy} g_{th} L_a = \alpha_{ia} L_a + \alpha_{ip} L_p + \ln\left(\frac{1}{R}\right), \tag{2.22}$$

where the mean mirror intensity reflection coefficient, $R = r_1 r_2$. For cleaved-facet lasers based upon GaAs or InP, $R \sim 0.32$. Dividing Eq. (2.22) by the total cavity length, L, realizing that $\Gamma_{xy} L_a / L \approx \Gamma_{xy} \Gamma_z = \Gamma$ (exact for $L_a \gg \lambda$), and defining the average internal loss $(\alpha_{ia} L_a + \alpha_{ip} L_p)/L$ as $\langle \alpha_i \rangle$ we have

$$\langle g \rangle_{th} = \Gamma g_{th} = \langle \alpha_i \rangle + \frac{1}{L} \ln\left(\frac{1}{R}\right). \tag{2.23}$$

For convenience the mirror loss term is sometimes abbreviated as, $\alpha_m \equiv (1/L)\ln(1/R)$. Noting that the photon decay rate, $1/\tau_p = 1/\tau_i + 1/\tau_m = v_g(\langle \alpha_i \rangle + \alpha_m)$, we can also write

$$\Gamma g_{th} = \langle \alpha_i \rangle + \alpha_m = \frac{1}{v_g \tau_p}. \tag{2.24}$$

As noted in Appendix 5, if the averaging is initially done over the whole volume, the three-dimensional modal gain and loss used in Eqs. (2.23) and (2.24) are obtained directly. However, this obscures the physics of the recirculating mode in the cavity, so we have chosen to show the longitudinal weighting separately here. As suggested above, the general $\langle g \rangle_{th}$ form is always valid, but the Γg_{th} form only should be used for in-plane lasers. The limitation that $L_a \gg \lambda$ for $L_a/L = \Gamma_z$ listed above is also discussed in Appendix 5. As explained there, the axial averaging of gain and loss must also use a weighted average over the axial standing wave pattern in the general case. In fact, for very short active regions ($L_a \ll \lambda$), such as in many vertical-cavity lasers, it is possible for $\Gamma_z \approx 2L_a/L$, if the active segment is placed at the peak of the electric-field standing wave (see Appendix 5).

It is important to realize that Eqs. (2.23) and (2.24) give only the cavity loss parameters necessary to calculate the threshold gain. They have nothing to do with the stimulated emission physics which determines what the gain is for a given injection current. This physics is briefly summarized in Appendix 6, and it will be the primary subject of Chapter 4.

For the phase part of Eq. (2.20), $\exp(2j\beta_{tha}L_a)\exp(2j\beta_{thp}L_p) = 1$, requires that $\beta_{tha}L_a + \beta_{thp}L_p = m\pi$, which gives a condition on the modal wavelength,

$$\lambda_{th} = \frac{2}{m}[\bar{n}_a L_a + \bar{n}_p L_p], \tag{2.25}$$

where m is the longitudinal mode number. It should also be realized that $\bar{n}$ varies with wavelength ($\partial\bar{n}/\partial\lambda$, dispersion), and it generally is also dependent upon the carrier density ($\partial\bar{n}/\partial N$, plasma loading). Thus, when making computations these dependences must be included. That is, to determine $\bar{n}$ at a wavelength $\lambda = \lambda_0 + \Delta\lambda$ and a carrier density, $N = N_0 + \Delta N$, we use

$$\bar{n}(\lambda, N) = \bar{n}(\lambda_0, N_0) + \frac{\partial \bar{n}}{\partial \lambda}\Delta\lambda + \frac{\partial \bar{n}}{\partial N}\Delta N. \tag{2.26}$$

Typically, $\partial\bar{n}/\partial\lambda \sim -1\ \mu\text{m}^{-1}$, and $\partial\bar{n}/\partial N \approx \Gamma_{xy}\partial n_A/\partial N \sim -\Gamma_{xy}10^{-20}\ \text{cm}^3$, where n_A is the index in the active region. Using Eqs. (2.25) and (2.26) we can find the wavelength separation between two modes, m and $m+1$, to be

$$\delta\lambda = \frac{\lambda^2}{2(\bar{n}_{ga}L_a + \bar{n}_{gp}L_p)}, \tag{2.27}$$

where the group effective index for the jth section, $\bar{n}_{gj} = \bar{n}_j - \lambda(\partial\bar{n}/\partial\lambda) = \bar{n}_j + \omega(\partial\bar{n}/\partial\omega)$. The group index in semiconductors is typically 20–30% larger than the index of refraction, depending on the specific wavelength relative to the band edge. From experiments, the values of $\bar{n}_g$ for the active sections of GaAs and InGaAsP DH in-plane lasers are near 4.5 and 4, respectively.

Finally, it is important to note that the steady-state gain in a laser operating above threshold must also equal its threshold value as given by Eq. (2.23). That is, *in a laser cavity*,

$$g(I > I_{th}) = g_{th}. \qquad \text{(steady state)} \tag{2.28}$$

If the gain were higher than g_{th}, then the field amplitude would continue to increase without bound, and this clearly cannot exist in the steady state. Furthermore, since the gain is monotonically related to the carrier density, this implies that the carrier density must also *clamp* at its threshold value. That is,

$$N(I > I_{th}) = N_{th}. \qquad \text{(steady state)} \tag{2.29}$$

In fact, what happens when the current is increased to a value above threshold is that the carrier density and gain initially (for on the order of a nanosecond) increase to values above their threshold levels, and the photon density grows. But then, the stimulated recombination term R_{st} also increases, reducing the carrier density and gain until a new steady-state dynamic balance is struck where Eqs. (2.28) and (2.29) are again satisfied. Put another way, the stimulated recombination term in (2.15) uses up all additional carrier injection above threshold. In terms of our reservoir analogy depicted in Fig. 2.2, the water level has reached the spillway and any further increase in input goes over the spillway without increasing the water depth. Of course, the spillway represents simulated recombination. Figure 2.7 shows the analogy in this case.

Figure 2.8 summarizes this carrier clamping effect in a laser cavity. The physics of the g vs. N curve never changes. The feedback effect causes the carrier density to clamp, in order to keep the gain at its threshold value.

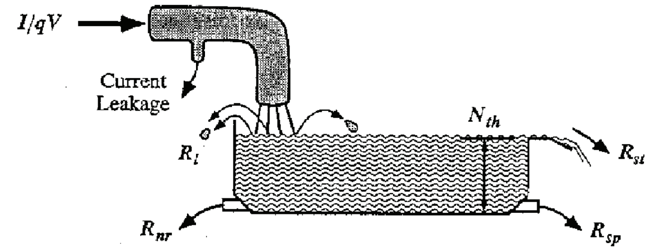

FIGURE 2.7 Reservoir analogy above threshold where water level has risen to the spillway so that an increased input results in an increased output (R_{st}) but no increase in carrier density (water level). The flows R_{nr} and R_{sp} do not change above threshold.

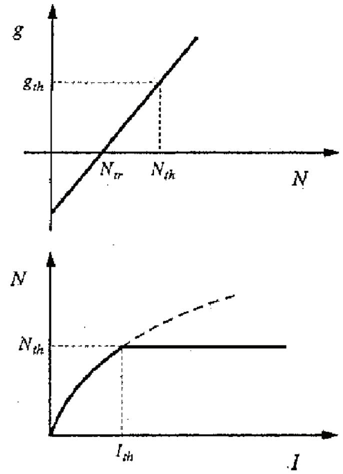

FIGURE 2.8 Gain vs. carrier density and carrier density vs. input current. The carrier density clamps at threshold causing the gain to clamp also.

2.6 THRESHOLD CURRENT AND POWER OUT VS. CURRENT

2.6.1 Basic *P–I* Characteristics

Although the rate equations (2.15) and (2.16) are valid both above and below threshold, we shall piece together a below-threshold LED characteristic with an above-threshold laser characteristic to construct the power out vs. current in for a diode laser. The LED part is already largely complete with Eq. (2.8). Thus, we shall here concentrate on the above threshold laser part. The first step is to use the below threshold steady-state carrier rate equation, Eq. (2.5) almost at threshold. That is,

$$\frac{\eta_i I_{th}}{qV} = (R_{sp} + R_{nr} + R_l)_{th} = \frac{N_{th}}{\tau}. \tag{2.30}$$

Then, recognizing that $(R_{sp} + R_{nr} + R_l) = AN + BN^2 + CN^3$ depends monotonically on N, we observe from Eq. (2.29) that above threshold $(R_{sp} + R_{nr} + R_l)$ will also clamp at its threshold value, given by Eq. (2.30). Thus, we can substitute Eq. (2.30) into the carrier rate equation, Eq. (2.15), to obtain a new above-threshold carrier rate equation,

$$\frac{dN}{dt} = \eta_i \frac{(I - I_{th})}{qV} - v_g g N_p, \qquad (I > I_{th}) \tag{2.31}$$

where we have assumed η_i is not a function of current above threshold. From Eq. (2.31) we can now calculate a steady-state photon density above threshold where $g = g_{th}$. That is,

$$N_p = \frac{\eta_i (I - I_{th})}{q v_g g_{th} V}. \qquad \text{(steady state)} \tag{2.32}$$

Now with some relatively straightforward substitutions, we can calculate the power out, since it must be proportional to N_p. To obtain the power out, we first construct the *stored optical energy in the cavity*, E_{os}, by multiplying the photon density, N_p, by the energy per photon, $h\nu$, and the cavity volume, V_p. That is, $E_{os} = N_p h\nu V_p$. Then, we multiply this by the *energy loss rate through the mirrors*, $v_g \alpha_m = 1/\tau_m$, to get the optical power output from the mirrors,

$$P_0 = v_g \alpha_m N_p h\nu V_p. \tag{2.33}$$

Substituting from Eqs. (2.32) and (2.24), and using $\Gamma = V/V_p$, in Eq. (2.33),

$$P_0 = \eta_i \left(\frac{\alpha_m}{\langle \alpha_i \rangle + \alpha_m} \right) \frac{h\nu}{q} (I - I_{th}). \qquad (I > I_{th}) \tag{2.34}$$

Now, by defining

$$\eta_d = \frac{\eta_i \alpha_m}{\langle \alpha_i \rangle + \alpha_m}, \tag{2.35}$$

we can simplify Eq. (2.34) to be

$$P_0 = \eta_d \frac{h\nu}{q} (I - I_{th}). \qquad (I > I_{th}) \tag{2.36}$$

Equation (2.36) represents the total power out of both mirrors. If the mirrors have equal reflectivity, then exactly half will be emitted out of each. If one is totally reflecting, then all will be emitted out the other. On the other hand, if the mirrors have partial but unequal reflectivity, the fraction emitted from each is a nontrivial function which we shall derive in Chapter 3. Equation (2.36) also shows that the power out above threshold is a linear function of the current above threshold. This is true regardless of our assumptions about the form of the gain–current relationship or the nature of the nonradiative recombination mechanisms. The assumptions necessary for this P–I linearity are that the gain–current relationship, the internal efficiency, the confinement factor, and the cavity losses remain constant. As shown in Appendix 5, by confinement factor, we really mean that the *modal gain* must remain constant.

To determine what we should call η_d, we can compare the calculated result of Eq. (2.36) to a measurement. Postulating that it might be related to a quantum efficiency, we calculate a differential quantum efficiency, defined as the number of photons out per electron in from a measured P–I characteristic. As shown in Fig. 2.9, the differential quantum efficiency would be found by measuring the slope $[\Delta P_0/\Delta I]$ in watts/amp above threshold (including output from both ends) and then multiplying this number by $[q/h\nu]$ in Coulombs/joule to get an empirical number of photons per electron equal to $[\Delta P_0/\Delta I][q/h\nu]$. Now, if we take the derivative with respect to current of Eq. (2.36), and solve for η_d, we get the same result. This shows that η_d is indeed *the differential quantum efficiency*. To repeat then,

$$\eta_d = \left[\frac{q}{h\nu} \right] \frac{dP_0}{dI}. \qquad (I > I_{th}) \tag{2.37}$$

The region in Fig. 2.9 below threshold $(I < I_{th})$ can be approximated by neglecting the stimulated emission term in Eq. (2.16) and solving for N_p, again

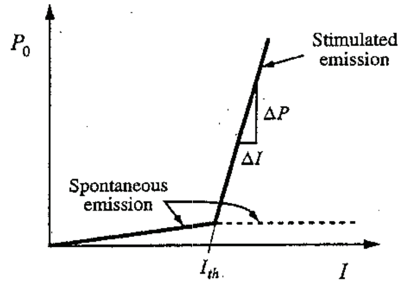

FIGURE 2.9 Illustration of output power vs. current for a diode laser. Below threshold only spontaneous emission is important; above threshold the stimulated emission power increases while the spontaneous emission is clamped at its threshold value.

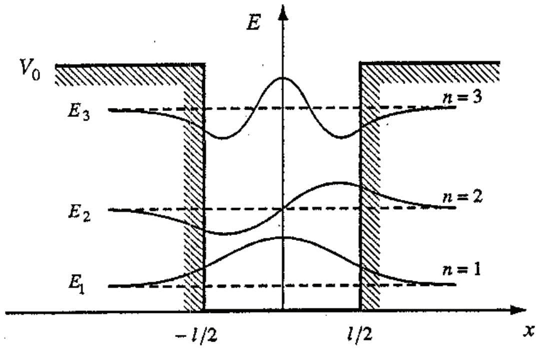

FIGURE A1.2 Energy levels and wavefunctions of one-dimensional potential well. Three bound solutions illustrated.

integral of the product of a wavefunction times its own complex conjugate is unity, then the wavefunctions would be *orthonormal.*

To determine the bound solutions, we need to solve the characteristic equations. For infinitely large V_0, such that the wavefunction goes to zero at the boundaries, i.e., $\psi(l/2) = 0$, the characteristic equation for both symmetric and antisymmetric cases becomes simply

$$\frac{kl}{2} = \frac{n\pi}{2}, \qquad n = 1, 2, 3, \ldots \tag{A1.13}$$

where odd (even) quantum numbers correspond to symmetric (antisymmetric) states. The corresponding discrete energy levels in terms of the quantum numbers are

$$E_n = n^2 E_1^\infty, \tag{A1.14}$$

where

$$E_1^\infty = \frac{\hbar^2 k_1^2}{2m} = \frac{\hbar^2\pi^2}{2ml^2} = 3.76(m_0/m)(100\ \text{Å}/l)^2 \quad \text{in meV.}$$

When V_0 is reduced from infinity, the discrete energies can still be found using (A1.14), however, the quantum numbers in this case are no longer simple integers, but are real numbers which we will refer to as n_{QW}. For example, if $V_0 = 25E_1^\infty$, the infinite-barrier integer quantum numbers $n = 1, 2, 3, 4, 5$ become $n_{QW} = 0.886, 1.77, 2.65, 3.51, 4.33$.

To calculate n_{QW} for an arbitrary V_0, we need to solve the characteristic equations given in Eqs. (A1.11) and (A1.12). Using Eq. (A1.14), combined with the definitions for k and γ given below Eqs. (A1.8) and (A1.9), the characteristic equations can be conveniently normalized:

$$\tan\left[\frac{\pi}{2} n_{QW}\right] = \frac{1}{n_{QW}} [n_{max}^2 - n_{QW}^2]^{1/2} \qquad \text{(symmetric)} \tag{A1.15}$$

$$\tan\left[\frac{\pi}{2} (n_{QW} - 1)\right] = \frac{1}{n_{QW}} [n_{max}^2 - n_{QW}^2]^{1/2} \qquad \text{(antisymmetric)} \tag{A1.16}$$

where

$$n_{QW} \equiv \sqrt{\frac{E_n}{E_1^\infty}} \quad \text{and} \quad n_{max} \equiv \sqrt{\frac{V_0}{E_1^\infty}}. \tag{A1.17}$$

These equations can be solved graphically by plotting both the left-hand side (LHS) and the right-hand side (RHS) as a function of n_{QW}. Figure A1.3 illustrates this procedure for four different values of V_0.

Note that only a finite set of quantum numbers exist for a given potential barrier, V_0. The normalized variable, n_{max} when rounded up to the nearest integer, yields the largest number of bound states possible for a given V_0. For example, with $V_0 = 3E_1^\infty$, from Eq. (A1.17), we find that $n_{max} = \sqrt{3} \approx 1.73$. Thus, only two bound states are possible under these circumstances. This is perhaps demonstrated more clearly by plotting the possible n_{QW} as a continuous function

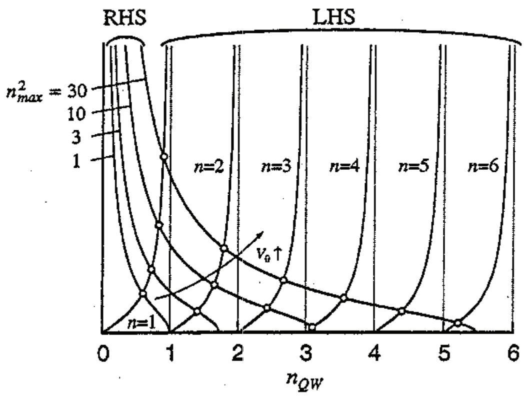

FIGURE A1.3 Graphical solution to Eqs. (A1.15) and (A1.16). The intersections between the LHS and RHS of the equations yield the possible values of n_{QW} for a given n_{max} (or equivalently V_0). The odd (even) quantum numbers displayed next to each tangent curve correspond to the LHS of the symmetric (antisymmetric) characteristic equation.

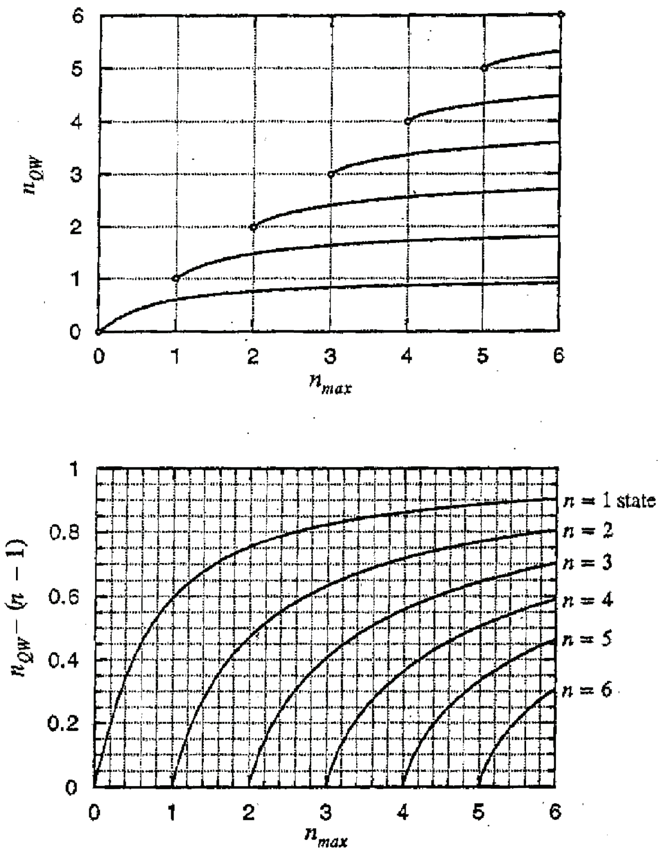

FIGURE A1.4 Plot of quantum numbers as a function of the maximum allowed quantum number which is determined by the potential height, V_0. The quantum numbers are related to V_0 and E through Eq. (A1.17). The lower plot gives a close-up view of the curves (which have been shifted vertically to fit on the same scale).

of n_{max}. Figure A1.4 gives all possible solutions for $n_{max} \le 6$ (which covers nearly all practical ranges of interest). Note that all quantum numbers approach their integer limit as n_{max} increases toward infinity. In addition, the quantum numbers cease to satisfy the equations (indicated by the open circles) when a given quantum number approaches the integer value of the next lowest state. The lowest quantum number can be approximated to within ±1% using the following formula:

$$n_{QW} \approx \frac{2}{\pi} \tan^{-1}[n_{max}(1 + 0.6^{n_{max}+1})]. \tag{A1.18}$$

A1.2 ELEMENTS OF SOLID-STATE PHYSICS

A1.2.1 Electrons in Crystals and Energy Bands

Electrons in crystals experience a periodic potential originating from the regularly spaced wells at the lattice ions. Figure A1.5 gives a schematic picture along one dimension of such a lattice. As predicted in Chapter 1, when N_A atoms are coupled in such a manner, each atomic energy level of the constituent atoms splits into a *band* of N_A discrete levels. However, this splitting is only significant for the uppermost energy levels where the two atoms interact.

There are several approaches that have been applied to solve this problem. The Kronig–Penney model approximates the actual periodic potential of Fig. A1.5 by a square wave potential, then uses the single rectangular well solution above as a starting point. However, the result is a complex transcendental equation that must be solved numerically. A second approach which provides better closed-form analytic solutions is the coupled-mode approach of Feynman et al. [1]. For accuracy some fairly complex functions need to be evaluated, but by leaving them in general form, we can still get a good picture of the nature of the solutions.

The first step is to go back to Schrödinger's equation and consider a possible general solution for a perturbed system, such as the atom which has been placed into a crystal. The isolated atom had a set of orthonormal wavefunction

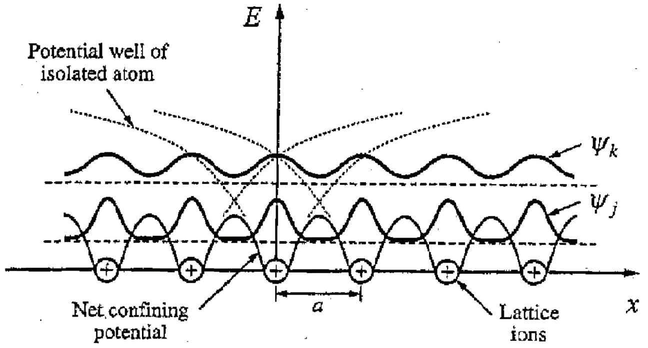

FIGURE A1.5 Schematic of net potential variation along a one-dimensional crystal lattice. Wavefunctions of nominally bound (ψ_j) and free (ψ_k) electron states are illustrated.